PREMIER COLLOQUE IMAGE
Traitement, Synthèse, Technologie et Applications
BIARRITZ — Mai 1984 —



# Tomographic Image Reconstruction from a Limited Number of Projections
# Reconstruction Tomographique avec un Nombre Limite de Projections

A. G. Lindgren

Electrical Engineering Department,
University of Rhode Island, Kingston, Rhode Island 02881

P. A. Rattey

Raytheon Submarine Signal Division, Portsmouth, RI 02871

## RESUME

Abstract:

This paper addresses the reconstruction of a function from its rectangularly sampled Radon transform. The Radon transform sampling requirements are reviewed and a convolution/backprojection reconstruction algorithm is described. Two basic issues are addressed. First, it is shown that even when the Radon transform of an image is adequately sampled (in the Nyquist sense), the standard convolution/backprojection algorithm may lead to a poor reconstruction unless the Radon transform is first reconstructed to a required set of projections. Secondly, when the Radon transform is undersampled in projections, reconstruction approaches are illustrated which span the range from those which achieve a high uniform-resolution reconstruction with large amounts of aliasing artifacts to those which achieve a low nonuniform-resolution reconstruction with virtually no aliasing artifacts. Reconstruction filters which seek a compromise between those two extremes are defined.

## I. Introduction

Image formation is an efficient means of displaying data derived from measurements and of conveying vast amounts of information rapidly. Since its introduction, computed tomography has revolutionized areas of science where the instrument of imaging was previously unavailable. In spite of the different physical situations which give rise to tomographic imaging problems, all share certain similar mathematical features. In particular, in each case the 2-D measurement process can be viewed as a system with an associated measurement operator S. This operator maps a bivariate slice function f (assumed here to be continuously defined over a domain D in the xy plane, see Fig 1) into a discrete set of measurements:

$$f(x,y) \xrightarrow{S} \{z_k,\ k = 1, 2, \ldots, K\} \qquad (1)$$

Very often the transformation (after perhaps some preprocessing) can be reasonably well approximated by a linear integral transformation:

## SUMMARY

$$z_k = \iint_D f(x,y) S_k(x,y)\,dx\,dy \qquad (2)$$

In this paper attention is focused onto a standard tomographic imaging problem [1-12] which is concerned with reconstructing f(x,y) from a set of (parallel-beam) projections that are uniformly spaced in angle over $2\pi$ radians, see Fig. 1. Data aquisition is typically expensive, both literally and in terms of invasion of the subject under study. This often results in a sampling grid that is sparse. A commonly encountered situation involves image reconstructions from a limited number of projections. This problem is the focus of this paper. Since measurements at a fixed value of $\theta$ are relatively inexpensive we shall assume that the sampling in the u-direction along each projection is adequately dense. The consequences of undersampling in the u-direction have been discussed previously [8,9] and the insights gained there can be extended to the current work. The basic approach taken in this paper relies heavily on multidimensional signal theory and signal processing techniques [13-15].

## II. The Reconstruction Problem and the Rectangularly Sampled Radon Transform

Consider the case where each measurement is an integral of f(x,y) over a line in the xy plane defined by

$$x \cos\theta_m + y \sin\theta_m = u_n \qquad (3)$$

Under these conditions the measurement $p(\theta_m, u_n)$ is a sample of the ($\theta$u - coordinatized) continuous Radon transform [6] defined by

$$p(\theta,u) = R[f(x,y)] = \iint_D f(x,y)\,\delta(u - x\cos\theta - y\sin\theta)\,dx\,dy \qquad (4)$$

where $\delta(u)$ is a Dirac delta function. A more standard tomographic imaging problem involves a uniformly spaced set of projection measurements where each measurement is an integral of f(x,y) over a strip in the xy plane as shown in Fig. 2.

In this case the resulting measurement function $p(\theta_m,u_n)$, defined on a discrete set of points $(\theta_m,u_n)$, provides a uniform sampling of a blurred or smoothed version of the Radon transform of the (continuous) slice function f(x,y) [9]. This 2-D sequence of points in the θu-plane is referred to as the rectangularly sampled Radon transform and is illustrated in Fig. 3. Thus, the measurement process maps the continuously defined bivariate function f(x,y) into a discretely defined 2-D sequence function p(mΔθ, nΔu); i.e.,

$$f(x,y) \xrightarrow{S} p(m\Delta\theta,\ n\Delta u) \qquad (5)$$

The fundamental objective of the imaging problem is to reconstruct f(x,y) (or at least an approximation to it) from its rectangularly sampled Radon transform. The basic philosophy of our approach involves a reconstruction of the Radon transform from the measurements followed by an appropriate inversion algorithm on the reconstructed Radon transform. For a large class of problems, when measurement blurring occurs it represents a space-invariant smoothing of the Radon transform. This is efficiently handled in the Radon transform domain by standard signal processing techniques [9,10,15]. The restored (deblurred) Radon transform is then inverted to reconstruct f(x,y). This approach, avoids the difficulties and complexity of deblurring in the image space where the effects of the measurement blurring may be space varying [9,11,16]. Consequently, for simplicity in the development presented in the following sections, we assume that the (unblurred) Radon transform is directly measured.

## III. Sampling the Radon Transform

For a slice function f with compact support on a disk of radius R, the Radon transform is restricted to a strip of width 2R, see Fig. 4b, and is periodic in θ with period 2π. Rattey and Lindgren have shown that under these conditions the band region of $P(w_\theta, w_u)$, the two-dimensional Fourier transform of $p(\theta,u)$ for arbitrary f(x,y), is fan (or bowtie) shaped and its approximate boundary (see [7,8] for a detailed discussion on the boundary of the band region) satisfies

$$P(w_\theta,w_u) \cong 0 \text{ for } |w_\theta| > R|w_u| + 1 \qquad (6)$$

If f(x,y) is effectively frequency limited to a W-disk, as in Fig. 4c, then the Fourier transform of the Radon transform also satisfies

$$P(w_\theta,w_u) \cong 0 \text{ for } |w_u| > W \qquad (7)$$

and $P(w_\theta, w_u)$ is supported only on an RW-bowtie as shown in Fig. 4d. (This bandregion shape means that the minimal (Nyquist) sampling of the Radon transform is achieved with a hexagonal sampling of the θu-plane [8,17]. Here however we focus only onto the more standard rectangular sampling grid which is most commonly studied.) Clearly, for the rectangularly sampled Radon transform, aliasing is avoided (see Fig. 5), if the sample grid spacing in Fig. 3 satisfies

$$\Delta u < \pi/W \qquad (8)$$

and

$$\Delta\theta < \pi/(RW+1) \qquad (9)$$

This means that in order to avoid aliasing when imaging an arbitrary object the number of projections, M, of f(x,y) effectively spanning 2π radians must satisfy

$$M = \frac{2\pi}{\Delta\theta} > 2(RW+1). \qquad (10)$$

Because of symmetry, these M projections spanning 2π radians can actually be obtained with only M/2 projections spanning π radians [9,10].

The approximation of (6) is an upper bound on the band region of the Radon transform of f(x,y). For certain special functions, this band region boundary is pessimistically large [8-12]. For instance, the Radon transform of a circularly symmetric function has a band region confined solely to the $w_u$ axis, i.e., $P(w_\theta, w_u) = 0$ for $w_\theta \neq 0$. Thus, (10) is a sufficient but not a necessary sampling condition. It is shown later, however, that when sampling is more sparse than (10) special precautions must be taken if an inverse Radon transform (convolution-backprojection) approach to reconstruction is taken. Basically it is shown that it is desirable to fill in missing views so that (10) is satisfied.

If the Radon transform for these special objects is bandlimited in the θ direction to $M_b \leq RW + 1$, i.e.,

$$P(w_\theta, w_u) \cong 0 \text{ for } |w_\theta| > M_b \qquad (11)$$

then to avoid aliasing the spacing between projections must satisfy

$$\Delta\theta < \pi/M_b \qquad (12)$$

or the number of projections M effectively spanning 2π radians must satisfy

$$M > 2M_b \qquad (13)$$

It is again pointed out that these M projections spanning 2π radians can actually be obtained with only $M/2 > M_b$ projections spanning π radians.

## IV. Reconstruction When Adequately Sampled in Parallel-Beam Projections

A discrete series representation of f based on an exact continuous representation of f via the inverse Radon integral transformation is developed in [12]. There it was shown that if the sampling requirements of (8) and (9) are met, then the continuous convolution-backprojection approach to the inverse Radon transform defined by

$$f(x,y) = R^{-1}[p(\theta,u] = \frac{1}{2\pi}\int_0^{2\pi} \tilde{p}\ (\theta,\ x\cos\theta + \sin\theta)\ d\theta \qquad (14a)$$

where

$$\tilde{p}(\theta,u) = p(\theta,u) * h(u) \qquad (14b)$$

and

$$h(u) = \frac{1}{4\pi}\int_{-W}^{W} |w_u| \exp(jw_u u)\ dw_u \qquad (14c)$$

can be transformed to the equivalent discrete series expansion

$$f(x,y) = \frac{1}{M_r}\sum_{m=0}^{M_r-1}\sum_{n=-\infty}^{\infty} \tilde{p}(m\Delta\theta, n\Delta u) \cdot \text{sinc}\left((\pi/\Delta u)(n\Delta u - (x\cos m\Delta u + y \sin m\Delta u))\right) \text{rect}\left((x^2+y^2)^{1/2}/R\right) \quad (15a)$$

where

$$\text{sinc}(x) \triangleq \sin x/x \quad (15b)$$

$$\text{rect}(x) \triangleq \begin{cases} 1 & \text{if } |x| > 1 \\ 0 & \text{otherwise} \end{cases} \quad (15c)$$

and $M_r$, the number of projections (over $2\pi$ radians) required for reconstruction, must satisfy

$$M_r > M_b + RW + 1 \quad (15d)$$

In (15) rect $(\sqrt{x^2+y^2}/R)$ windows the reconstruction to the original R-disk, and $\tilde{p}(m\Delta\theta, n\Delta u)$ is the filtered Radon transform ($p(m\Delta\theta, n\Delta u)$ obtained by a discrete convolution which is equivalent to the "magnitude-omega" filtering of (14b)). Modified versions of the magnitude-omega are employed to deblur measurements and smooth measurement noise [9,11,18]. The reconstruction achieved by this approach (assuming the space and frequency support requirements are met) is exact to within the accepted accuracy of sampling theory. In practice, the sinc basis (interpolation) functions are replaced by simpler basis functions [11]. For example, the algorithm used for this work first zero-pads and then low pass filters $\tilde{p}(m\Delta\theta, n\Delta u)$ in the u-direction so that the sampling spacing in the u-direction is reduced to $\Delta u/8$. This more densely sampled $\tilde{p}$ is then used in (15a) with simple linear 2-point connector basis functions.

If the projection sampling requirement (13) is satisfied and if there are fewer projections then required for reconstruction ($M < M_r$), then all $M_r$ projections can (and must) be obtained by low-pass filtering the M-projection sampled Radon transform in the $\theta$ direction. The reason $M_r$ projections are required for reconstruction can be understood by an examination of (15a) which is recast in a slightly different form below:

$$f(x,y) = \frac{1}{2\pi}\int_0^{2\pi}\int_{-\infty}^{\infty} \tilde{p}_d(\theta, u)\, \delta(u)\, du\, d\theta \quad (16)$$

where

$$\tilde{p}_d(\theta,u) \triangleq \tilde{p}(\theta, u' + x\cos\theta + y\sin\theta) \quad (17)$$

represents a distortion of the convolved function $p(\theta,u)$ of (14b). The effect of this distortion is to spread the band region of $p(\theta,u)$ so that

$$\tilde{P}_d(w_\theta, w_u) \cong 0 \text{ for } |w_\theta| > M_b + \left(|w_u\sqrt{\tfrac{2}{x}+\tfrac{2}{y}}| + 1\right) \quad (18)$$

By Parseval's theorem (16) can be rewritten as

$$f(x,y) = \frac{1}{(2\pi)^2}\int_{-\infty}^{\infty}\int_{-\infty}^{\infty} \tilde{P}_d(w_\theta, w_u)\, \delta(w_\theta)\, dw_u\, dw_\theta \quad (19)$$

$$= \frac{1}{(2\pi)^2}\int_{-\infty}^{\infty} \tilde{P}_d(0, w_u)\, dw_u$$

Thus, when interpreted in the $w_\theta w_u$-plane, reconstruction of the function f at the point (x,y) involves integrating $\tilde{P}_d(w_\theta, w_u)$ along the $w_u$-axis [9,12]. Therefore, when concerned with the rectangularly sampled Radon transform, attention focuses onto whether or not aliasing of the $w_u$-axis occurs, see Fig (6). When reconstructing f to an R-disk, $\tilde{P}_d(w_\theta, w_u)$ is bandlimited in the $\theta$-direction to $M_b + (RW+1)$ (see (18)). Therefore, it is clear that the required number of projections needed to avoid aliasing the data along the $w_u$-axis must satisfy (15d).

To illustrate, for the case of a circularly symmetric object ($M_b = 0$) one view (projection) is sufficient to sample the Radon transform. However, to adequately backproject this object requires (RW +1) views. In this case the missing views $p(\theta,u)$ are filled in by duplicates of the convolved (magnitude-omega filtered) version of the one measured projection. With these added views included, the back-projection algorithm provides a reconstruction that is exact to within the accuracy of sampling theory. It is intuitively pleasing that the number of views depends on object (or viewing region) size and the object bandwidth (i.e., the space-bandwidth product.

In summary, for the discrete inverse Radon transform method of reconstruction, $M_r$ views are required for backprojection. These can be generated by standard signal processing techniques such as zero padding the measurements (i.e., filling in the missing views with zeros) and low pass filtering $p(\theta_m, u_n)$ to reduce the bandwidth to M/2. This converts the original M projections to $M_r$ projections. In the algorithm used in this paper $M_r$ is set to the nearest power of 2 greater than 2(RW +1) views, where $W = \pi/\Delta u$. These $M_r$ views are always generated from the M measured projections. Thus, the algorithm is universally applicable to objects that meet the designed space-bandwidth product. If $M > 2M_b$ then all is well and a good reconstruction results. If this criterion is not met then the proposed algorithm is one of several that reasonably treats the data when undersampled in projections.

## V Reconstruction when Undersampled in Parallel-beam Projections

When imaging an arbitrary slice function whose Radon transform bandregion is shown in Fig. (4), undersampling in the number of views leads to aliasing as shown in Fig. (7). A more detailed discussion including other (e.g. fan beam) sampling geometries is available in references [8,12].

The reconstruction described in the previous section corresponds to filtering away all information for $|w_\theta| > M/2$ see Fig (8a). Alternative approaches would include the anti-aliasing filter shown in Fig. (8b). This filter rejects all aliased information without regard to relative amounts of aliased to nonaliased information. This results in a reconstruction with no aliasing artifacts. The price paid for the rejection of these artifacts is a loss of resolution. In fact, a variable resolution

reconstruction is obtained with twice the resolution at the center as at the edge of the R-disk reconstruction [8,9,11,19]. Another approach is one which retains all the original information and accepts the aliasing. When reconstructing only within the R-disk, this filter passband is shown in Fig. (8c). This type of filtering is automatically invoked through the inversion process. Hence, this result is the same as merely processing the available views in the convolution-backprojection algorithm. In one sense the filter of Fig. (8a) represents a compromise between the extremes of Fig (8b and 8c).

Another approach to reconstruction when undersampled in views involves a minimum variance filter that weights the available frequency information by the "signal to signal-plus-noise" ratio, where the aliasing is considered to represent noise. This approach has been pursued in [11] where a generally applicable minimum variance filter was designed based on a spectral density model which uniformly weights all spatial components of an image over an R-disk. In the absence of a priori spectral density information, this filter can be used. It has been demonstrated by experiment that this filter (Fig. 8d) produces optimum SNR reconstructions. Obviously, endless variations are possible and optimal designs require a priori information regarding the object distribution and spectral properties [11,15]. For the general imaging problem (where f(x,y) is arbitrary) the filters described here are practical and of interest in actual imaging situations. We believe, the viewpoint outlined here and detailed in [9,11] provides a point of view and insight not previously available in tomographic problems and gives the researcher an approach to the imaging problem that permits specialized processing algorithms to be conceived.

## VI. Experimental Results and Discussion

An imaging system based on 39 samples per projection and 64 projections (128 over $2\pi$ radians) is employed throughout this section. This system is nominally designed to handle objects scaled to fill the circular viewing region with a space-bandwidth product $2RW = 38\pi$.

Reconstruction is accomplished as described in [11]. This requires interpolation of $p(\theta_m, u_n)$ in the u-direction for each of 128 views and evaluation of the sum over $\theta$ as defined in (15). Since the series representation (15) permits f(x,y) to be reconstructed continuously over the R-disk, the slice function is reconstructed on a 128x128 grid.

To illustrate the results obtained in section V, the Fresnel pattern (defined by $f(x,y) = \cos(k(x^2+y^2))$ is reconstructed to test the imaging system. This pattern has a spectrum $F(w_x, w_y)$ that is essentially flat out to a cut-off frequency defined by the width of the outer ring, see the Fresnel-zone plate of Fig. (9a). The reconstruction is shown in Fig (9b). For an downsampling in $\theta$ by a factor of eight (leaving 8 views over $\pi$ radians) a reconstruction using the convolution-backprojection approach on the available views is shown in Fig (9c) and artifacts are clearly visible. Since 8 views are more than adequate to represent $p(\theta,u)$ for this circularly symmetric object, these errors are due to aliasing of the $w_u$ axis by the distorted function (17) that arises during the back-projection phase of the reconstruction process. By low pass filtering $p(\theta_m, u_n)$ in the $w_\theta$ direction, the missing (zero-padded) views are filled in avoiding the above aliasing and resulting in the reconstruction of Fig. (9d).

To illustrate the anti-aliasing and minimum variance filters referred to in section V, the cross-section function of Fig. (10a) was reconstructed from a limited number of projections. This slice function is comprised of three impulses convolved with a Gaussian point spread function to "effectively" limit the support of $F(w_x, w_y)$ to a W-disk where $W = \pi/\Delta u$. A reconstruction with the required number (128 views over $2\pi$ radian) of views duplicates this function with acceptable error [11]. Reconstructions under a down-sampling in $\theta$ by a factor of 8 are shown in Figs. (10b-e) for standard convolution-backprojection of the available views, anti-aliasing filter, the minimum variance filter, and also a filter which simply limits the $\theta$ bandwidth to M/2, respectively. For these filters the missing views are replaced by zeros (zero-padded) and the interpolation resulting from the filtering operation fills the 128 x 39 grid for $p(\theta,u)$. Interpolation in the u-direction is as described in [11]. As predicted in [9,11], when the anti-aliasing filter of Fig. (8b) is employed, the resolution at the center of the viewing region is twice that at the edge, see Fig. (10c). For the standard convolution-backprojection reconstruction, the artifacts (mainly streaks) are quite dramatic (see Fig. 10c). This streaking, due to aliasing, is essentially removed in the reconstruction of Fig. (10c). However, the original object has a substantial loss of resolution because of the anti-aliasing filtering operation. Because the anti-aliasing filter virtually eliminates the aliasing artifacts the presence of the lower amplitude impulse is clearly evident in this reconstruction (in spite of its loss of resolution), whereas it is more difficult to spot in the other reconstruction. The reconstructions using the minimum variance filter, and the filter which simply cuts off at $|w_\theta| = M/2$ see Figs. (10d and e), strike a compromise between the reconstructions of Figs. (10b) and (10c).

## VII Conclusion

This paper has focused on the standard tomographic imaging problem of reconstructing a function from its rectangularly sampled Radon transform. The basic philosophy of the approach presented here first involves reconstruction of the Radon transform to a required set of projections using standard multi-dimensional signal processing techniques. This is followed by the convolution/backprojection inversion algorithm.

We have shown that even when the Radon transform of an image is adequately sampled (in the Nyquist sense, i.e. (13) is satisfied), the standard convolution/backprojection reconstruction algorithm will generally lead to poor reconstruction unless the Radom transform is first reconstructed to a sufficiently dense set of projections. A simulation example was presented to illustrate this point. We then went on to show that when the Radon transform is undersampled, various reconstruction options are available. Blind application of the standard convolution/backprojection algorithm in this situation yields a high (uniform) resolution reconstruction with a large amount of aliasing artifacts present. On the other extreme is an anti-aliased reconstruction which has virtually no aliasing artifacts but has poor (nonuniform) resolution. Other filtering methods which fill in missing projections seek a compromise between

these extremes by trading off resolution for aliasing artifacts.

Although we describe in this paper only the convolution/backprojection inversion algorithm and modified versions of it, elsewhere [12] we have compared this reconstruction approach with a Hilbert-space approximation approach. The latter encompasses the approach using natural pixels taken by Buonocore, Brady, and Macovski[20], and the approach using a degrees of freedom analysis taken by McCaughey and Andrews [21]. We found that this alternate approach, applied to the rectangularly sampled Radon transform achieves reconstructions which lie between those of the anti-aliased and the blind convolution/backprojection filters of Fig. 8b and 8c. While the convolution/backprojection approach and the Hilbert-space approximation require similar processing, the former is simpler and provides more insight into the imaging problem. Thus the results and methods presented here are especially important in the field of tomographic image reconstruction when measurements represent a rectangular sampling of the Radon transform.

Acknowledgement:

The authors wish to express their appreciation to Professor Robert Kelley, Director of the Robotics Research Center, for generously providing the facilities of the Vision Laboratory. We also wish to thank Ying Sun for interfacing the described reconstruction package with the vision facilities, and Bruce Smith for the extensive computer studies conducted on the various reconstruction algorithms.

References:

[1] J. Radon, "Uber die bestimmung von funkltiones durch ihre intergralwerte langs gewissen manigfaltigkeiten," Berichte Saechsische Akademie der Wissenschaften, vol. 69, pp. 262-277, 1917.

[2] A. Macovski, Medical Imaging Systems, Prentice Hall, 1983.

[3] R. N. Bracewell, "Strip integration in radio-astronomy," Astrophysics, J., vol. 150, pp. 427-434, 1967.

[4] R. A. Crowther, D. J. DeRosier, and A. Klug "The reconstruction of a three-dimensional structure from projections and its application to electron microscopy," Proc. Roy. Soc. Lond. A., vol. 317, pp. 319-340, 1970.

[5] A. M. Cormack, "Sampling the Radon transform with beams of finite width," Phys. Med. Biol., vol. 23, no. 6, pp. 1141-1148, 1978.

[6] G. N. Houndsfield, "Computerized transverse axial scanning (tomography): Part 1, description of the system," Brit. J. Radiol., vol. 46, pp. 1016-1022, 1973.

[7] H. J. Scudder, "Introduction to computer aided tomography," Proc. IEEE, vol. 66, no. 6, pp. 628-637, 1978.

[8] P. A. Rattey and A. G. Lindgren, " Sampling the 2-D Radon transform," IEEE Trans. ASSP, vol. 29, no. 5, pp.994-1002, 1981.

[9] A. G. Lindgren and P. A. Rattey, "The inverse discrete Radon transform with applications to tomographic imaging using projection data," in Advances in Electronics and Electron Physics, vol. 56, C. Marton, Ed. New York; Academic Press, pp. 359-410, 1981.

[10] P. A. Rattey and A. G. Lindgren, "Sampling the 2-D Radon transform with parallel and fan-beam projections," tech. rep. Dept. Electrical Engineering, University of Rhode Island, Kingston, 1980.

[11] P. A. Rattey, "Two-dimensional signal processing and the Radon transform," M.S.E.E. thesis, University of Rhode Island, Kingston, 1980.

[12] P. A. Rattey, "Tomographic image reconstruction from a limited number of projections." Ph.D. thesis, Dept. of Electrical Engineering, University of Rhode Island, Kingston, 1983.

[13] A. V. Oppenheim and R. W. Schafer, Digital Signal Processing, Prentice Hall, Englewood Cliffs, New Jersey, 1975.

[14] R. M. Mersereau and A. V. Oppenheim, "Digital reconstruction of multidimensional signals from their projections," Proc. IEEE, vol. 62, no. 10, pp. 1319-1338, 1974.

[15] H.C. Andrews and B. R. Hunt, Digital Image Restoration, Prentice Hall, New Jersey, 1977.

[16] J. G. Verly and R. N. Bracewell, "Blurring in tomograms made with x-rays of finite width," J. Comput. Assist. tomogr., vol. 3, no. 5, pp. 662-678, Oct. 1979.

[17] R. M. Mersereau, " The processing of hexagonally sampled two-dimensional signals," Proc. IEEE, vol. 67, no. 6, pp. 930-949, 1979.

[18] I. S. Reed, W. V. Glenn, C. M. Chang, T. K, Thruong, and Y. S. Kwoh, "Dose reduction in x-ray computed tomography using a generalized filter," IEEE Trans. Nucl. Sci., vol. NS-26, no. 2, pp. 2904-2907, 1979.

[19] A. Klug and R. A. Crowther, "Three-dimensional imge reconstruction from the viewpoint of information theory," Nature, vol. 238, pp. 435-440, 1972.

[20] M. H. Buonocore, W. R. Brady, A. Macovski, "A natural pixel decomposition for two-dimensional image reconstruction," IEEE Trans. Bio. Eng., Vol. BME-28, No. 2, pp. 69-78, 1981.

[21] D. G. McCaughey, and H. C. Andrews, "Degrees of freedom for projection imaging," IEEE Trans. Acoust., Speech, Signal Processing, Vol. ASSP-25, No. 1, pp. 63-73, 1977.

A.G. Lindgren and P.A. Rattey
Reconstruction Tomographique avec un Nombre Limite de Projections
Tomographic Image Reconstruction from a Limited Number of Projections

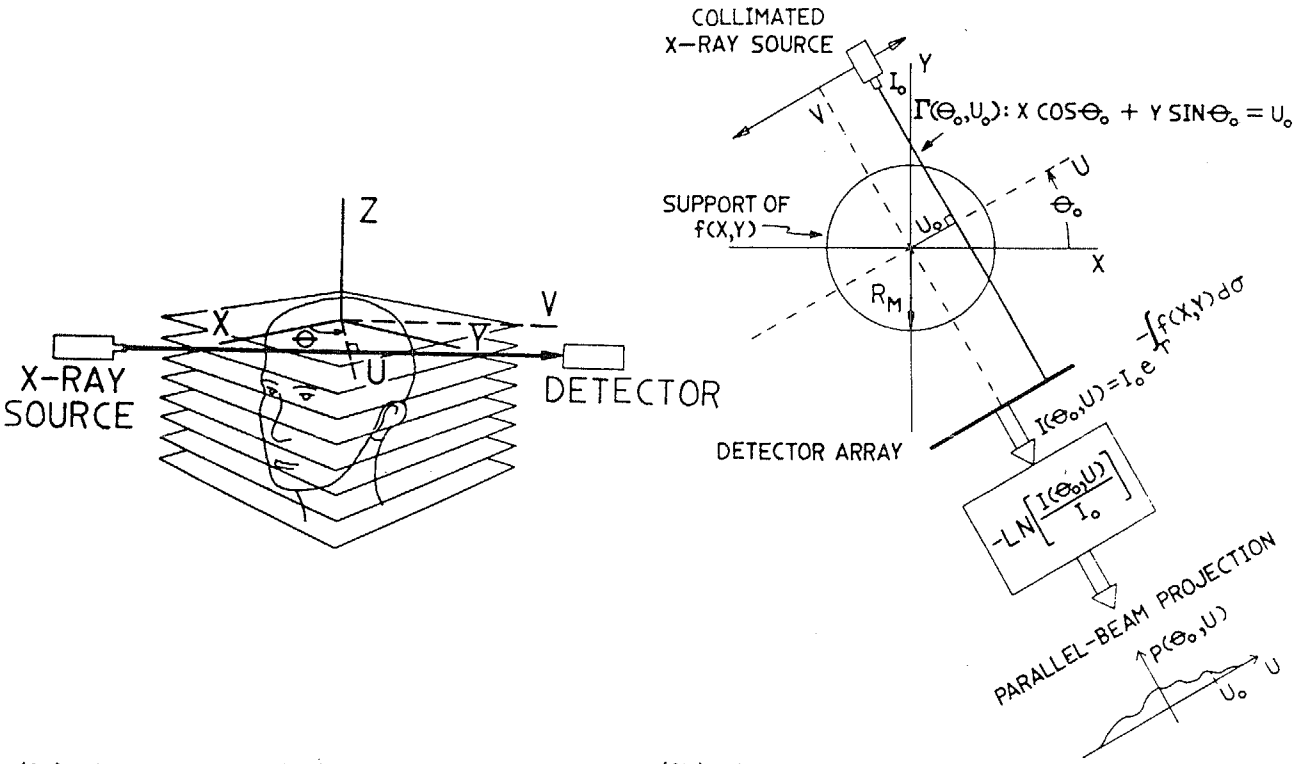


(1a) In x-ray transmission tomography, a three-dimensional object is decomposed into a set of parallel slices or cross-sections. An x-ray beam is passed through a particular slice, and the attenuated beam intensity is measured as it exits the head. Each measurement, defined by the coordinates $\theta$ and u, is exponentially related to the integral of the slice (cross-section) attenuation function over the line defined by the beam path.

(1b) In parallel-beam geometry, for a fixed orientation angle $\theta_o$, x-rays from a collimated source (which translates in the u-direction) are attenuated as they pass through a cross-section of an object (characterized by f(x,y)). This gives rise to the attenuated intensity measurement function $I(\theta_o,u)$, for all u. The (logarithmic) transformed measurement function, $p(\theta_o,u)$, a parallel-beam projection, is then computed. This provides samples of the $\theta$u-coordinitized Radon transform for a particular $\theta=\theta_o$:

Fig. 1 X-ray transmission tomography employing parallel-beam geometry.

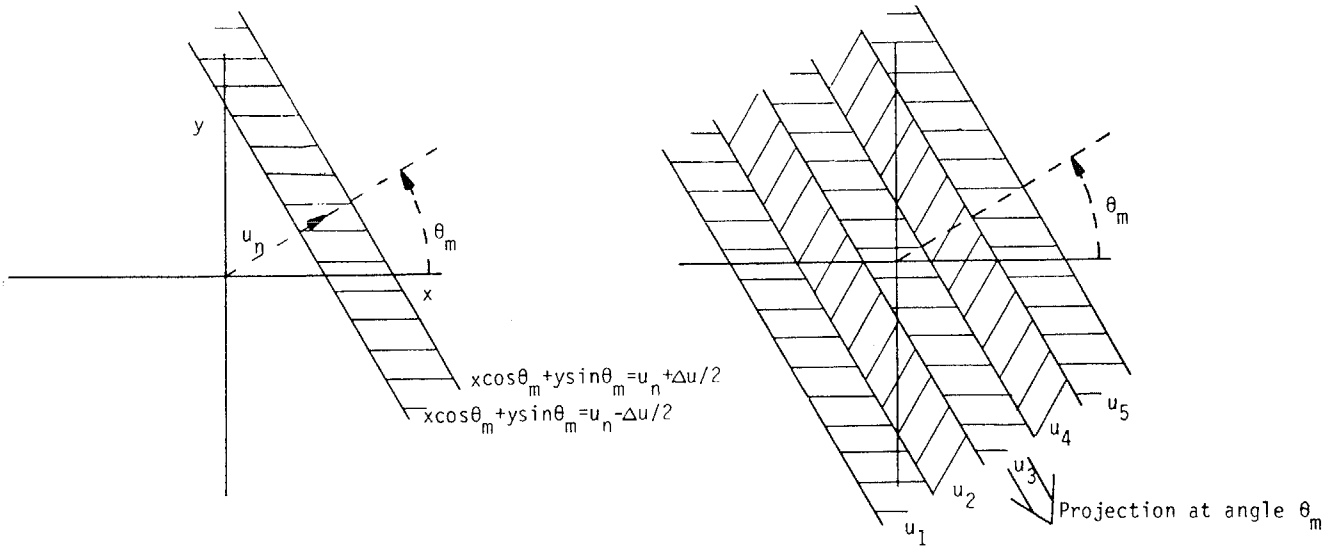


Figure 2a. Rectangular integration strip at a signed distance $u_n$ from origin and angle $\theta_m$.

2b. Set of contiguous integration strips leading to a parallel-beam projection of f.

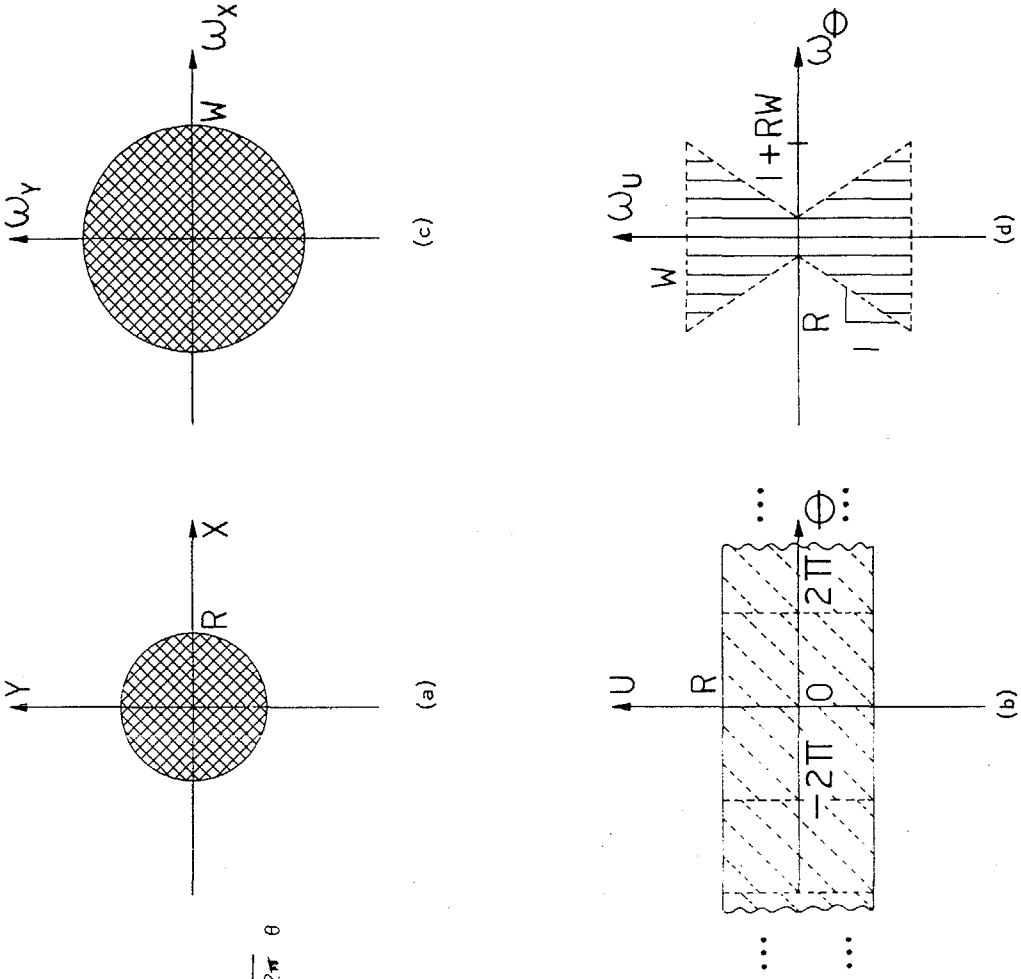


Fig. 4 Regions of support for various related functions
a) R-disk support of f (x,y)
b) Support region of p(θ,u), the Radon transform of f(x,y) in (a)
c) W-disk support of F ($w_x$, $w_y$) the Fourier transform of f(x,y) in (a)
d) Support region of P ($w_\theta$, $w_u$), the 2-D Fourier transform of the Radon transform of f(x,y) satisfying (a) and (b)

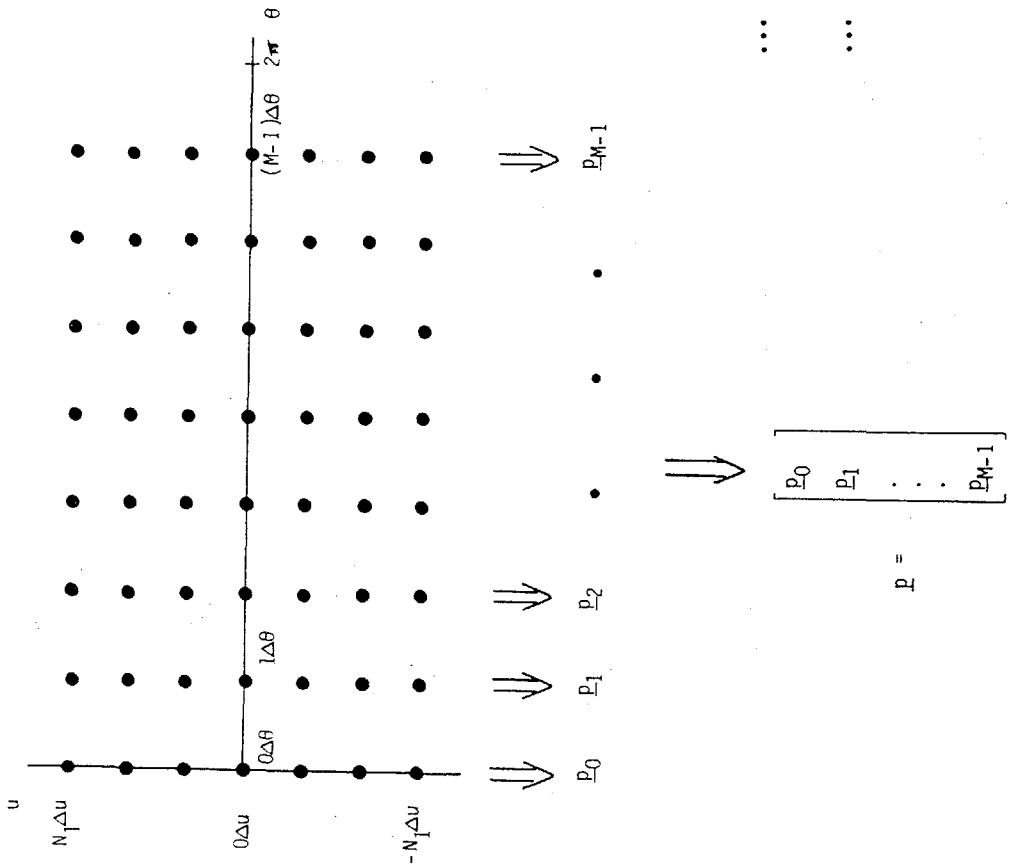


Figure 3. Rectangular sampling grid for one cycle of the Radon transform and the ordering of samples into a vector.

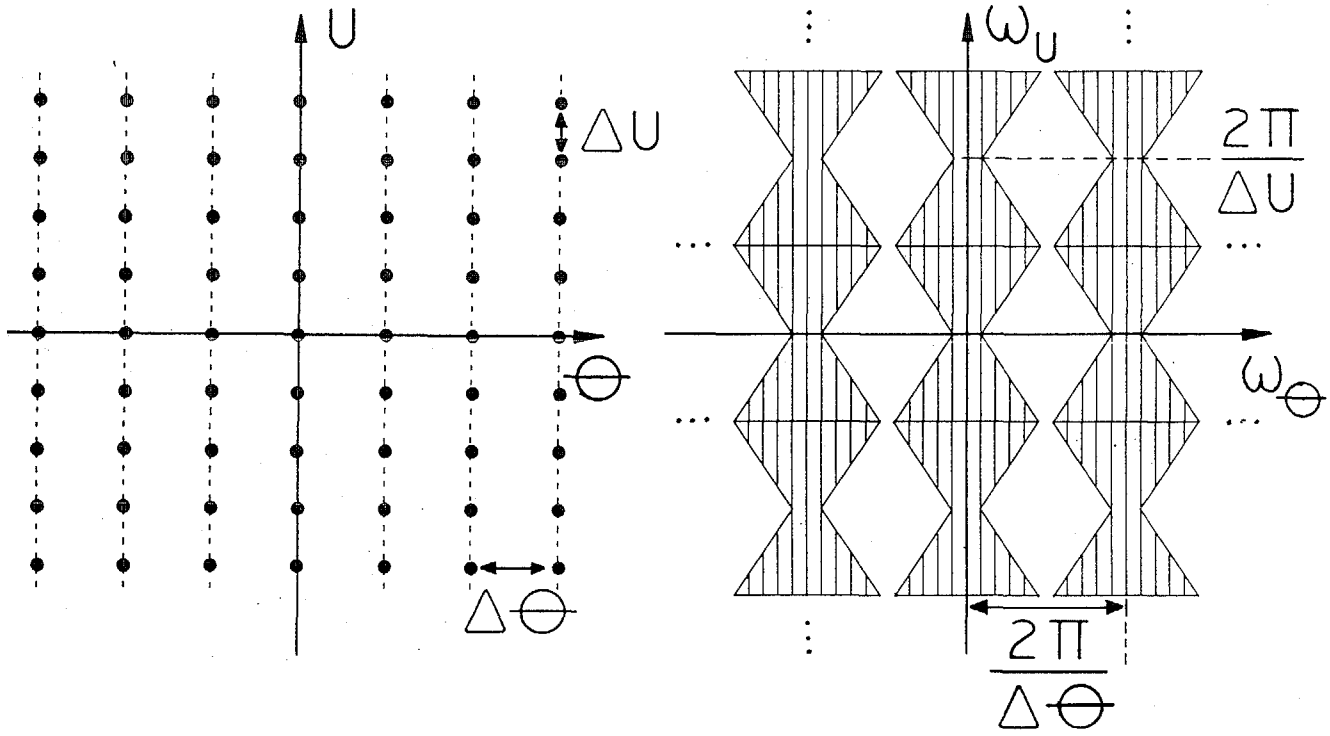


Fig. 5. Support of rectangularly sampled Radon transform (whose band region is shown in Fig. 4 (d)) and its Fourier transform.

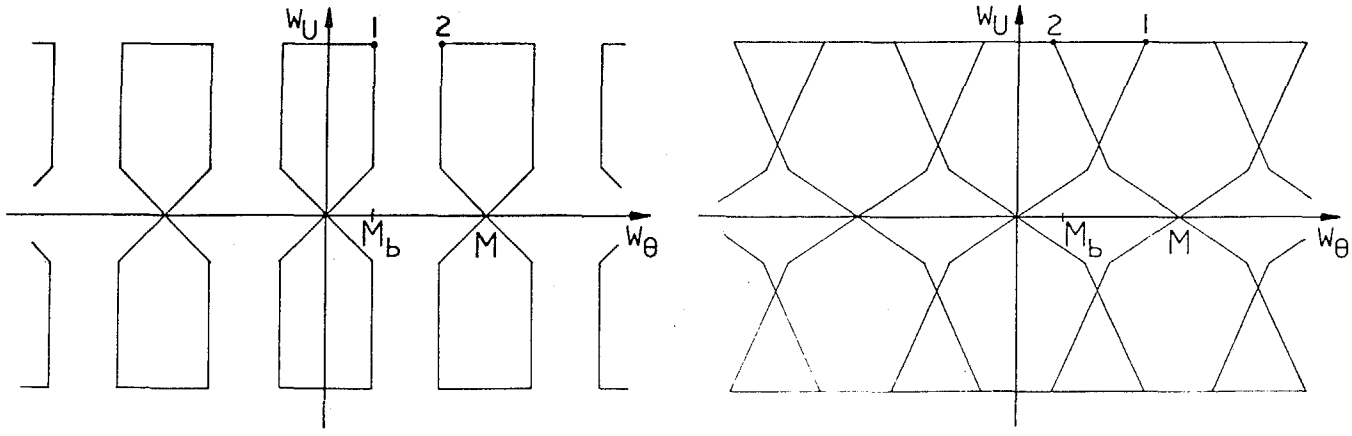


Fig. 6. Effect of distortion on bandregion of the $|w_u|$-filtered Radon transform (a) Bandregion of rectangular-sampled $p(\theta,u)$. Replication of baseband spectrum in the $w_\theta$-direction is caused by $\theta$-sampling. Sampling effects in the u-direction are not shown here. (b) Bandregion of the distorted function $p_d(\theta,u) = p(\theta,u + x\cos\theta + y\sin\theta)$. In (b), spreading of the bandregion in (a) occurs; aliasing will not affect reconstruction of $f(x,y)$ so long as point 2 does not migrate past the $w_u$-axis or equivalently point 1 (for which $w_\theta = M_b + Wr + 1$ (see (18))) does not migrate past the line $w_\theta = M$.

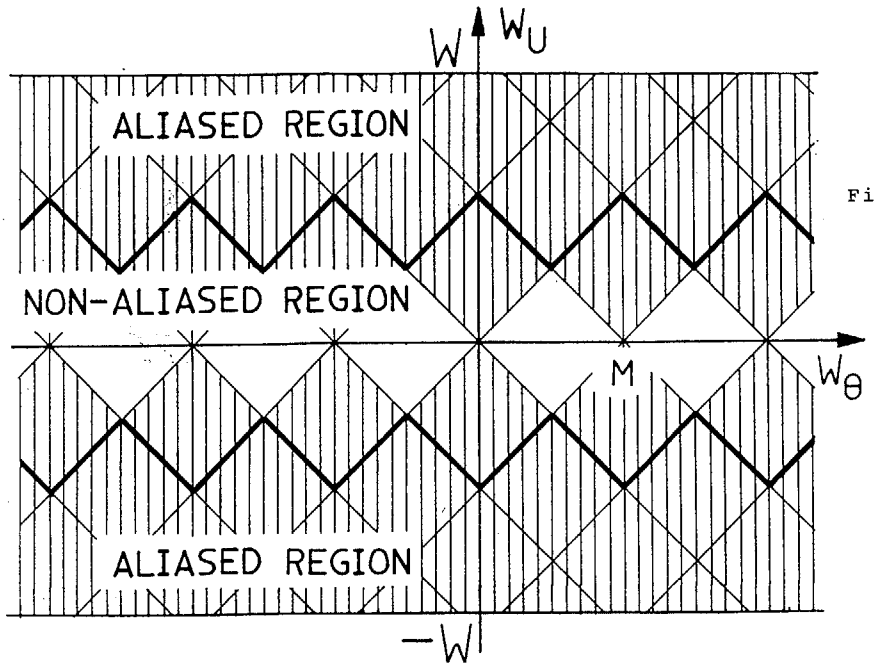


Fig 7 Support of $P(w_\theta w_u)$ the Fourier transform of the projection sampled Radon Transform $p(\theta,u)$ generated from M equispaced parallel-beam projections from 0 to $2\pi$. This band region represents a periodic replication of the RW-bowtie of Fig. 4d. Overlapping of translated bowtie band regions produces aliasing.

Fig. 8 Various lowpass filter passbands used in different proceesing algroithms when undersampled in projections (see Fig. 7)
(a) filtering away all information for $|w_\theta| > \frac{M}{2}$
(b) rejecting all aliased information
(c) retaining all available information
(d) Minimum-variance filter response

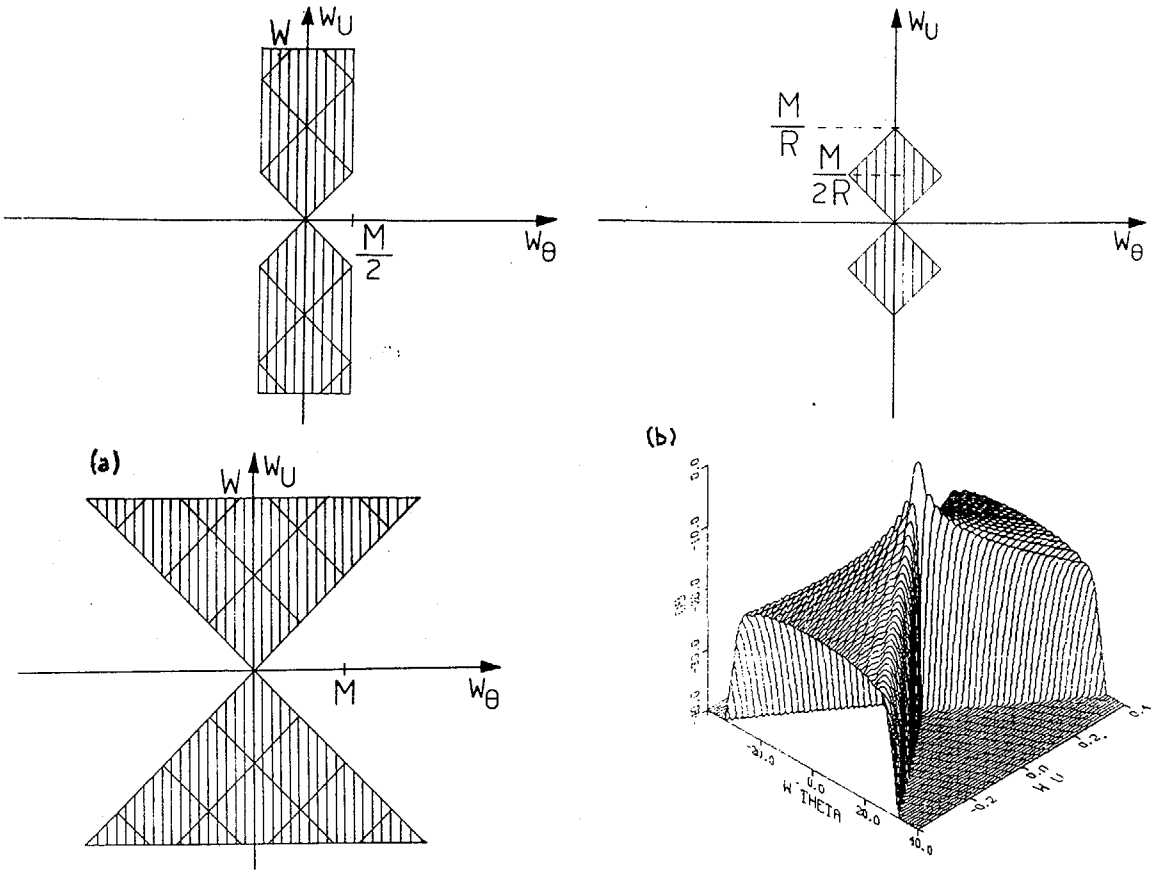


(c)

(d)

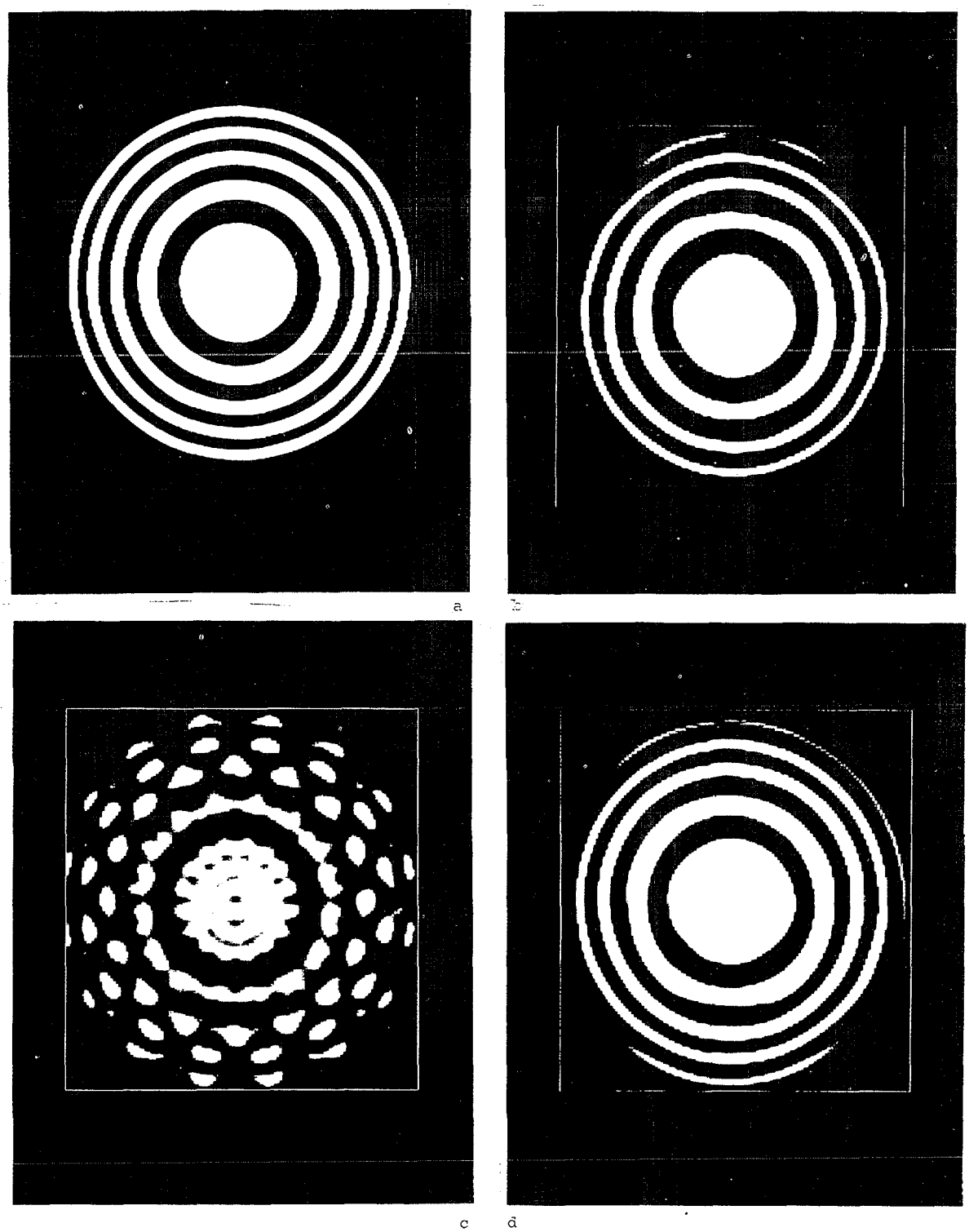


Fig. 9 Reconstruction of FRESNEL-ZONE PLATE image

a) Original Image
b) Reconstruction of FZP in Fig. 9a with full set of projections
c) Reconstruction of FZP in Fig. 9a using 1/8 the full set of projections and no lowpass filtering in θ-direction to fill in missing views.
d) Reconstruction of FZP in 9a as in Fig 9c except with lowpass filtering in θ-direction to fill in missing views.

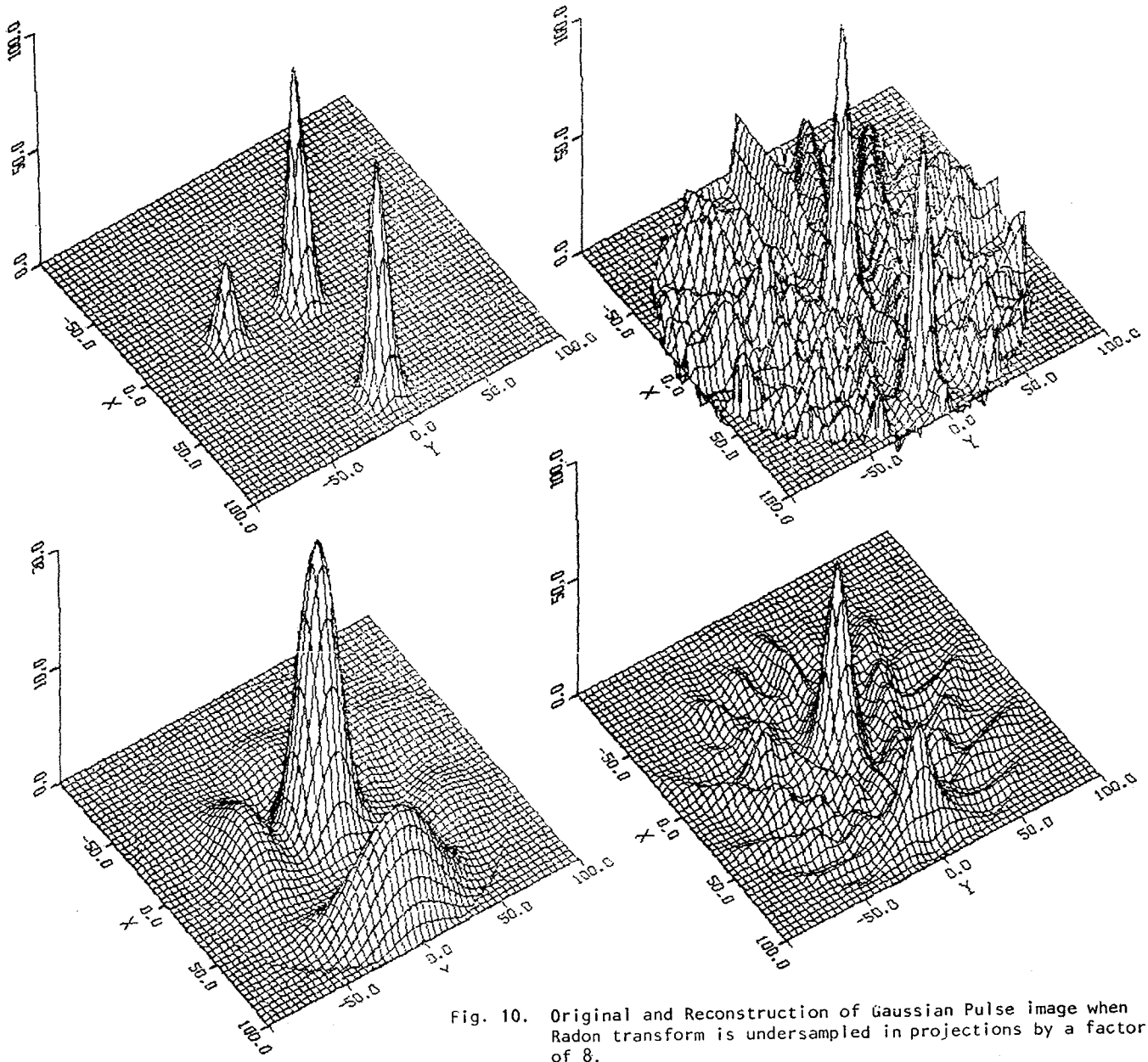


Fig. 10. Original and Reconstruction of Gaussian Pulse image when Radon transform is undersampled in projections by a factor of 8.

(a) Original image, reconstruction using full set of projections reproduces this image exactly.

(b) Standard convolution/backprojection reconstruction. Note the artifacts due to aliasing.

(c) Reconstruction using anti-aliasing filter. Note the rejection of aliasing artifacts and the nonuniform resolution.

(d) Reconstruction using minimum-variance filter.

e) Reconstruction using θ-lowpass filter with cutoff at $|W_\theta| = M/2$.